Contribution to the Special Issue "Electron transfer in coordination chemistry and molecular materials science"

A Zinc(II) Tetraphenylporphyrin Peripherally Functionalized with Redox-Active "*trans*-[(η^5-C_5H_5)Fe(η^5-C_5H_4)C≡C](κ^2-dppe)$_2$Ru(C≡C)-" Substituents: Linear Electrochromism and Third-Order Nonlinear Optics

Areej Merhi,[a,b] Guillaume Grelaud,[a,c] Nicolas Ripoche,[a,c] Adam Barlow,[c] Marie P. Cifuentes,[c] Mark G. Humphrey,*[c] Frédéric Paul*[a] and Christine O. Paul-Roth*[a,b]

[a] *Institut des Sciences Chimiques de Rennes, ISCR-UMR CNRS 6226, Université de Rennes 1, Campus de Beaulieu, 35042 Rennes Cedex, Rennes, France*

[b] *INSA-ISCR-UMR 6226, Université Européenne de Bretagne, INSA de Rennes, 35043 Rennes Cedex, France*

[c] *Research School of Chemistry, Australian National University , Canberra ACT 0200, Australia*

E-mail: christine.paul@univ-rennes1.fr or christine.paul@insa-rennes.fr

E-mail: frederic.paul@univ-rennes1.fr

E-mail: mark.humphrey@anu.edu.au

Dedicated to Dr Claude Lapinte on the occasion of his retirement, in fond memory of the good times spent together in France and Australia.

ABSTRACT

A nonametallic organometallic-coordination complex (**4**), assembled from redox-active ferrocenyl (Fc) and Ru(κ^2-dppe)$_2$ fragments (dppe = 1,2-bis(diphenylphosphino)ethane) as peripheral donor groups and a central Zn(II) tetraphenylporphyrin (ZnTPP) core, has been prepared and characterized. Complex **4** is obtained in one step from a pentametallic organometallic porphyrin precursor following substitution of the peripheral chloride ligands by ferrocenylalkynyl moieties (C≡CFc). The spectroelectrochemistry of **4**, and that of previously reported porphyrins featuring related peripheral electron-rich d^6-transition metal alkynyl units, has been investigated; the optical and redox properties of **4** are briefly discussed, and its potential, and that of a related pentanuclear tetraferrocenyl ZnTPP complex, to function as redox-switchable chromophores is examined. Preliminary studies of the cubic NLO properties of **4** have been undertaken by Z-scan studies at 560 nm and 630 nm, the results from which are also reported.

Keywords: Porphyrin; Alkynyl complex; Ferrocene; π-conjugation; Electrochromism; Nonlinear optics

1. Introduction

Materials with cubic nonlinear optical (NLO) properties are required for various applications in photonics, nanophotonics, and biophotonics [1-3]. The processing of optical signals such as ultrafast switching or modulation of optical beams using materials with sizeable third-order NLO responses is of significant interest [3-5]. Amongst the wide range of molecular chromophores investigated in the last 30 years, organometallic compounds have emerged as very promising building blocks to access new NLO-active materials [6-8], while the outstanding cubic NLO properties of porphyrins are also widely recognized [9-12]; in particular, several families of porphyrins with extended π-manifolds have been systematically screened for their large multiphoton absorption cross-sections in the visible/near-IR range [13,14]. Along the same lines, organometallic metal-alkynyl complexes were first investigated for their NLO responses in the mid-1980s [15]. These complexes allow for greater structural control and design than their purely organic counterparts, as the metal centre, oxidation state, ligation and, in some cases the geometry of the complex can be systematically varied [16-18]. Moreover, in specially designed dipolar electron-rich d^6 metal-alkynyl derivatives, the polarizable metal centre can act as a powerful donor group, affording access to multipolar organometallic architectures with redox-switchable NLO properties [19,20]. Indeed, due to the existence of kinetically stable oxidized state(s) with distinct NLO properties, redox-switching of the NLO behaviour has been demonstrated in several instances at selected wavelengths with these particular building blocks [21,22]. More recently, fluorescence has also been switched in a related Zn(II) diphenylporphyrin ([ZnDPP]) conjugate [23]. Peripheral functionalization of a Zn(II) tetraphenylporphyrin core by metal-alkynyl complexes was therefore envisioned as an attractive target.

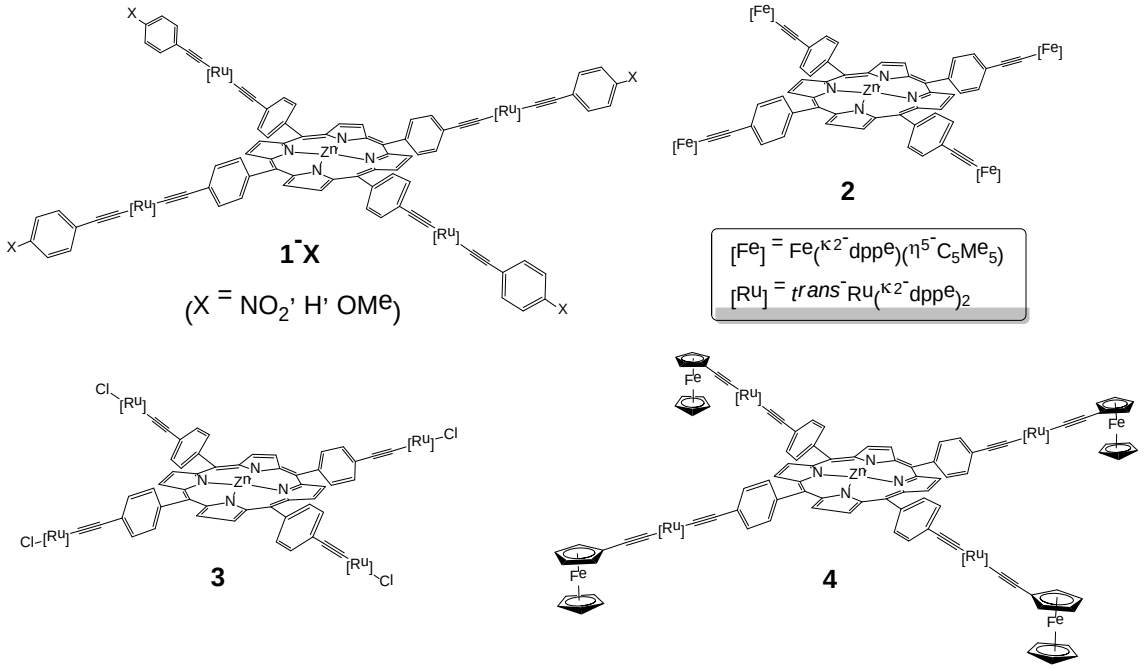

Scheme 1. Selected Organometallic Porphyrin Derivatives.

Accordingly, we have recently found that monomeric Zn(II) tetraphenylporphyrin (ZnTPP) derivatives functionalized by electron-rich metal alkynyl complexes, such as **1**-**X** and **2** (Scheme 1), exhibit strong cubic NLO activity at specific wavelengths in the visible/near-IR range, in particular large effective two-photon absorption (TPA) cross-sections in the range 700-750 nm [24,25]. We report herein UV-vis-NIR spectroelectrochemical data for **2** and **3**, as well as that of a new ZnTPP derivative **4**, obtained in one step from **3**, together with preliminary Z-scan studies on **4** at specific wavelengths. The potential of these compounds to exhibit redox-switchable NLO behaviour is briefly discussed, along with the impact of their structural differences on this remarkable property.

2. Experimental

2.1. General procedures

All reactions were performed using standard Schlenk techniques under argon with magnetic stirring [26]. Anhydrous CH_2Cl_2 was distilled from CaH_2 and sparged with nitrogen before use; all other solvents were HPLC grade and used as received. Commercially available reagents were

used without further purification unless otherwise stated. Na[PF_6] (Sigma-Aldrich) was recrystallized from MeCN.

^{1}H, ^{31}P and ^{13}C NMR spectra were recorded as $CDCl_3$ solutions using Bruker 200 DPX, 300 DPX and 500 DPX spectrometers. The chemical shifts are given in ppm and referenced to residual solvent peaks. The assignments were performed by 2D NMR experiments: COSY (Correlation Spectroscopy), HMBC (Heteronuclear Multiple Bond Correlation) and HMQC (Heteronuclear Multiple Quantum Coherence). IR spectra were recorded on Bruker IFS 28 spectrometer, using KBr pellets or in dichloromethane solution. UV-vis-NIR spectra were recorded on UVIKON XL (Biotek) and on Cary 5000 (Varian) spectrometers, while spectro-electrochemical experiments were performed using a homemade cell, as described below. Cyclic voltammograms were recorded at 25 °C in CH_2Cl_2 solutions (containing 0.10 M [*n*-Bu_4N][PF_6], purged with nitrogen and maintained under inert atmosphere) at 100 mV/s scan rate using an a e-corder 401 potentiostat system from eDaq Pty Ltd (using a Pt disk as working electrode, a Pt wire as counter-electrode and an Ag/AgCl reference electrode; $E° = -0.113$ V *vs.* SCE). The FcH/FcH^+ couple was used as an internal calibrant for the potential measurement (0.46 V *vs.* SCE, $\Delta E_p = 0.09$ V; $i_{pa}/i_{pc} = 1$) [27]. Elemental analyses were performed at the Microanalytical Service Unit at the Australian National University (ANU). High-resolution mass spectra were recorded on a ZabSpec TOF Micromass spectrometer in FAB mode or ESI positive mode in CH_2Cl_2/MeOH mixtures (9:1) at CRMPO in Rennes.

The porphyrin precursor 5,10,15,20-tetrakis{trans-[bis{bis(1,2-(diphenylphosphino)ethane}chlororuthenium(II)](4-ethynylphenyl)}porphyrinatozinc(II) (**3**) [25] and ethynylferrocene [28] were prepared according to literature methods.

*2.2. 5,10,15,20-tetrakis{trans-[bis{bis(1,2-(diphenylphosphino)ethane}(ferrocenylethynyl)-ruthenium(II)](4-ethynylphenyl)}porphyrinatozinc(II) (**4**)*

Triethylamine (0.15 mL) was added to a solution of 5,10,15,20-tetrakis{*trans*-[bis{bis(1,2-(diphenylphosphino)ethane}chlororuthenium(II)](4-ethynylphenyl)}porphyrinatozinc(II) (**3**) (0.12 g, 0.027 mmol), ethynylferrocene (0.030 g, 0.130 mmol) and Na[PF_6] (0.070 g, 0.420 mmol) in distilled CH_2Cl_2 (12 mL) under nitrogen. NEt_3 was added (0.3 mL, > 0.2 mmol) and the mixture was stirred 48 h at room temperature, the extent of reaction being monitored by ^{31}P NMR spectroscopy. The reaction mixture was then filtered, and the filtrate concentrated under

reduced pressure. The desired product was precipitated following addition to hexane, yielding the title compound as a green solid (0.09 g, 0.017 mmol). Yield: 63 %. Anal. calc. for $C_{308}H_{252}Fe_4N_4P_{16}Ru_4Zn$: C, 71.17; H: 4.89; N: 1.08; found: C: 70.89; H: 4.93; N: 1.31. HRMS-ESI (m/z): calcd for $[C_{308}H_{252}{}^{56}Fe_4N_4P_{16}{}^{102}Ru_4{}^{64}Zn]^{2+}$: 2598.4248, found: 2598.4312. FT-IR (*v*, KBr, cm^{-1}): 2052 (vs, RuC≡C). ^{1}H NMR (δ, 300 MHz, C_6D_6): 9.41 (s, 8H, H_{Pyr}), 8.40 (d, $^3J_{HH}$ = 8.1 Hz, 8H, H_{Ph}), 7.80 (m, 64H, $H_{Ph/dppe}$), 7.51 (d, $^3J_{HH}$ = 8.1 Hz, 8H, H_{Ph}), 7.15–6.90 (m, 96H, H_{Ph}), 4.27-4.12 (m, 36H, H_{Fc}), 2.70 (s, 32H, CH_2). ^{31}P{^{1}H} NMR (δ, 121 MHz, C_6D_6): 54.5 (s). ^{13}C{^{1}H} NMR (δ, 125 MHz, C_6D_6): 151.3 (s, $C_{\alpha\text{-pyrrolic}}$), 139.5 (s, C_{Ar}), 138.8 & 138.5 (m, $C_{ipso/dppe}$), 135.8 & 135.6 (s, $CH_{Ph/dppe}$ + CH_{Ar}), 132.8 (s, $C_{\beta\text{-pyrrolic}}$), 130.6 (s, C_{Ar}), 129.6 & 129.5 (s, $CH_{Ph/dppe}$), 128.7 (s, $CH_{Ph/dppe}$ partially hidden by solvent), 122.7 (s, C_{meso}), 117.7 (s, RuC≡*C*), 112.3 (s, RuC≡*C*), 78.0 (s, C_{Cp}), 69.9 (s, CH_{Cp}), 69.7 (s, C_5H_5), 67.2 (s, CH_{Cp}), 32.8 (m, $CH_{2/dppe}$); 2 Ru*C*≡C[C_f] and 1 CH_{Ar} not observed, possibly overlapped.

2.3. Spectroelectrochemistry

Solution UV-vis-NIR spectra of the oxidized species were obtained at 298 K or 248 K by electrogeneration on a platinum mesh electrode in a 0.5 mm optically transparent thin-layer electrochemical (OTTLE) cell [29], using a silver wire as pseudo-reference and a platinum wire as counter-electrode. Solutions were made up with 0.30 M [*n*-Bu_4N][PF_6] in dry and deoxygenated CH_2Cl_2 and kept under an atmosphere of pure nitrogen.

2.4. Z-Scan Measurements

Third-order nonlinear optical properties were investigated as previously described [25], but with some modifications. The laser system is housed in the Research School of Chemistry at the Australian National University and consists of a Quantronix Integra-C-3.5-F regenerative amplifier operating as an 800 nm pump and a Quantronix Palitra-FS BIBO crystal-based optical parametric amplifier. This system delivered wavelength tunable pulses of ~130 fs and was operated at a repetition rate of 1 kHz. Solutions of the compounds in dichloromethane of *ca.* 0.04 w/w% concentration were placed in 1 mm stoppered Starna glass cells; an identical cell was used for measurements of Z-scans on pure solvent. All measurements were calibrated by referencing to signals obtained from a fused silica plate with a thickness of 4.26 mm.

Experiments were performed at selected wavelengths (560 nm and 630 nm) by employing wavelength separators and colour glass filters to reject unwanted wavelengths. The pulse energy was attenuated to the μJ/pulse range, in order to maintain the nonlinear phase shifts obtained from the samples in the range *ca.* 0.3 -1.5 rad; this was then used as the excitation source for the simultaneous recording of open-aperture and closed-aperture Z-scan traces. The beam was focused to provide a focal spot with Gaussian beam waist $w_0 \approx 45$ - 60 mm (giving a Rayleigh length that was always sufficiently greater than the thickness of the cell or the reference silica plate, such that a "thin-sample" assumption was justified). The cuvette travelled on a motorized stage (Thor Labs) in the Z-direction, typically from –40 to 40 mm, and the data were collected using three InGaAs photodiodes (Thor Labs) that monitored the laser input, the open-aperture signal and the closed-aperture signal. The outputs were fed into three channels of a Rhode and Schwarz RTM1054 digital oscilloscope and the data were collected using custom LabVIEW software. The open- and closed-aperture traces obtained after dividing the corresponding signals by the laser input reference were analyzed with the help of a custom fitting program that used equations derived by Sheik-Bahae *et al.* [30]. The real and imaginary parts of the second hyperpolarizability, γ, of the solutes were then calculated assuming additivity of the nonlinear contributions of the solvent and the solute and the applicability of the Lorentz local field approximation [31]. The values of the imaginary parts of γ were also converted into values of the two-photon absorption cross-sections σ_2.

3. Results and Discussion

*3.1. Synthesis and Characterization of **4***

The new nonametallic porphyrin-based assembly was obtained in one step from the previously reported organometallic tetraruthenium-precursor **3** [25] and five equivalents of the ferrocenylalkyne [28]. The coupling proceeded *via* reaction conditions initially proposed by Touchard *et al.* for ruthenium alkynyl complex formation [32]. The reaction was monitored by ^{31}P NMR spectroscopy and was apparently complete after 48 h at room temperature. The desired nonametallic compound **4** was isolated by precipitation, resulting in its isolation in pure form in 63% yield (Scheme 2).

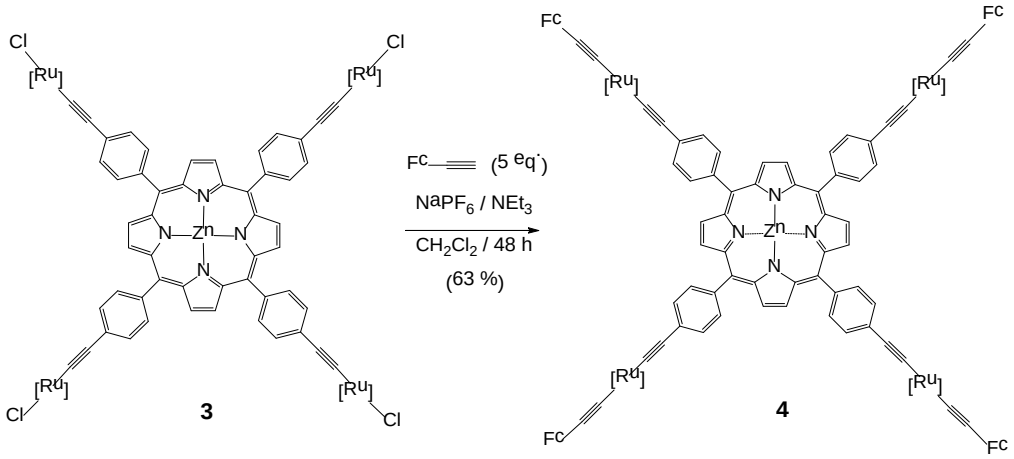

Scheme 2. Synthesis of **4**.

This new compound was fully characterized by means of microanalysis, electrospray ionization mass spectrometry (ESI-MS), IR, NMR, and UV-vis-NIR spectroscopies, and cyclic voltammetry (CV). A peak that can be assigned unambiguously to the molecular dication $\mathbf{4}^{2+}$ was observed by ESI-MS. The IR spectrum of **4** clearly reveals an intense $\nu_{C\equiv C}$ mode characteristic of σ-alkynyl ruthenium complexes around 2050 cm^{-1}[20,33-37]. As often observed [38], the stretching modes of the two distinct alkynyl ligands are not resolved in the infrared spectrum. The ^{31}P NMR spectrum shows a singlet corresponding to the equivalent phosphorus atoms from the dppe ligands, consistent with a fully symmetric derivative. Moreover, compared to the ^{31}P resonance of the precursor **3** at 51 ppm, the signal is shifted to lower field, around 54.5 ppm, as expected for a bis σ-alkynyl complex [39]. The symmetric functionalization of the porphyrin core in **3** is also confirmed by ^{1}H NMR spectroscopy, which shows a sharp singlet near 9.40 ppm corresponding to the eight equivalent β-pyrrole protons of the macrocyclic spacer. Furthermore, a multiplet in the correct ratio is observed near 4.25 ppm corresponding to the overlapped signals of the cyclopentadienyl protons of the terminal ferrocenyl moieties. Additional evidence for the proposed structure is seen in the ^{13}C NMR spectrum, despite the fact that the diagnostic quintuplets of the C_α alkynyl carbon atoms could not be detected [40,41].

Apart from slight shifts, the UV-vis spectrum of **4** strongly resembles that of **3**, with the two Q bands at 562 nm and 612 nm and the intense Soret band at 420 nm that are diagnostic of the porphyrin core (Fig. 1 and Table 1). This is unsurprising, because the ethynylferrocene fragment is usually poorly absorbing in the visible range ($\varepsilon < 2000$ $M^{-1}.cm^{-1}$) [42,43]. The weak

shoulder on the low-energy side of the Soret band is tentatively suggested to be associated with the new $d_{Ru \rightarrow} \pi^*_{TPP}$ MLCT bands [44].

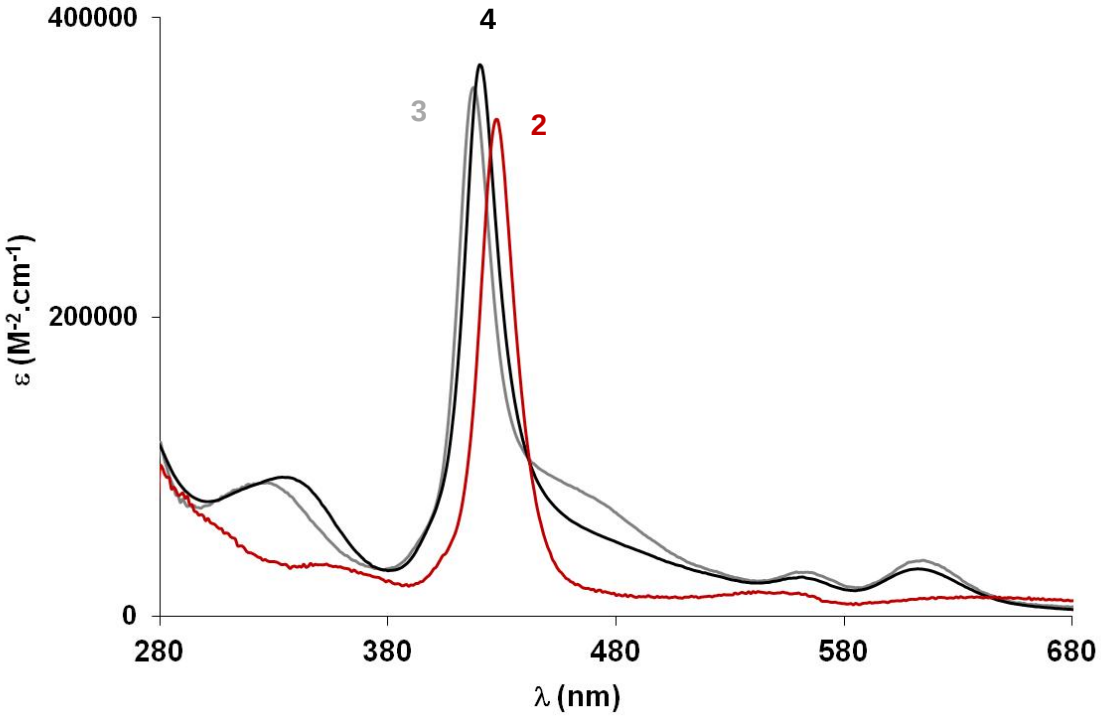

Fig. 1. UV-vis absorption spectra of the zinc porphyrins **2-4** in CH_2Cl_2 at 25 °C.

*3.2. Cyclic voltammetry study of **4***

The cyclic voltammetry (CV) study of **4** was performed in dichloromethane, with 0.1 M [*n*-Bu_4N][PF_6] as supporting electrolyte. When a solution of **4** is scanned over a small potential window (0.0 to 0.9 V) *vs.* SCE, two chemically reversible oxidation processes are seen at 0.18 V and 0.76 V, corresponding formally to the Fe(II)/Fe(III) and to the Ru(II)/Ru(III) oxidations, respectively (Fig. 2) [20,35,43,45]. There is a slightly larger peak-to-peak separation for the oxidation process of **4** at 0.86 V (90 mV), because it likely coincides with the (weaker) first oxidation process of the ZnTPP core, predicted to occur in the same potential range [25,46]. The oxidation of the Fe(II) centers in **4**, while taking place at higher potentials than in **2**, does however occur at significantly lower values than in ferrocene, due to the presence of proximal electron-rich Ru(κ^2-dppe)$_2$ groups. Conversely, oxidation of the Ru(II) centers occurs at significantly higher potentials that in the precursor compound **3** [25], due to the existence of a sizeable electronic coupling between these redox-active groups [33].

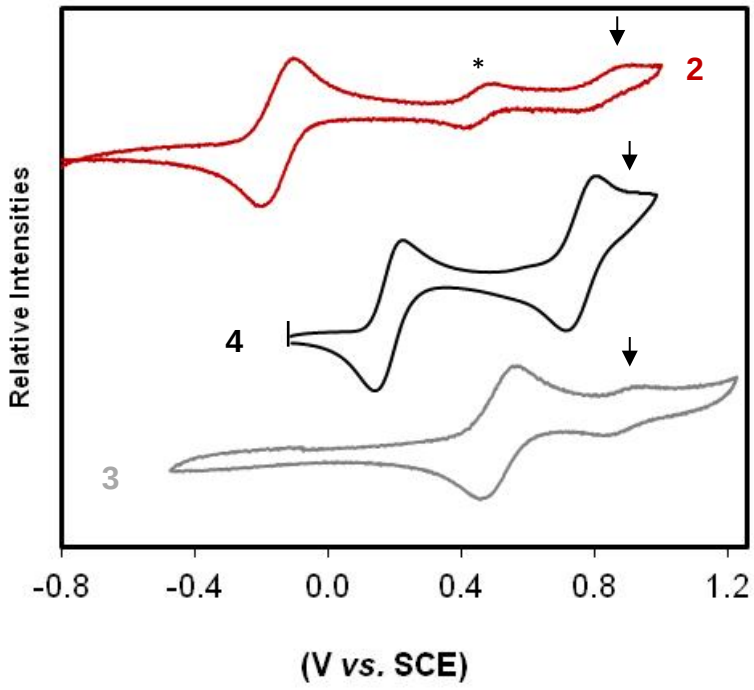

Fig. 2. Cyclic voltammogram of the zinc(II) porphyrins **2-4** in CH_2Cl_2/[*n*-Bu_4N][PF_6] (0.1 M) at 25 °C at 0.1 V/s between -0.8 and 1.2 V *vs.* SCE, showing the Fe- (left) and Ru-centered (right) oxidations. The ZnTPP-based oxidations are indicated by an arrow, while the asterisk indicates the FcH/FcH^+ couple (0.46 V) used as an internal calibrant.

When the potential window is expanded to -1.8 /1.6 V (Supporting Information), the two formally metal-centred redox events become irreversible while two additional (irreversible) oxidation processes can be observed at more positive potentials (around 1.2 V and 1.4 V *vs.* FcH^+/FcH). The first of these is significantly less intense than the Fe and Ru oxidation waves, and possibly corresponds to the second monoelectronic oxidation of the ZnTPP core of **4** [25]. The second additional oxidation wave, near 1.4 V, has a comparable intensity to the metal-centered processes observed at lower potentials, and might therefore be associated with a process taking place on the four Fe(III) or Ru(III) centers. Employing a less positive switching potential or increasing the scan rate did not render the second ZnTPP oxidation chemically reversible, consistent with a large kinetic instability associated with the nominally decacationic species $\mathbf{4}^{10+}$ at the electrode that results from the mono-oxidation of the eight Fe(II) and Ru(II)

metal centers followed by the di-oxidation of the porphyrin core. Its pronounced instability is not very surprising. Indeed, we have already observed in several instances that dicationic [FcC≡CRu(κ^2-dppe)$_2$C≡C-]$^{2+}$ fragments are not particularly kinetically stable in solution [20,33]. Increasing the oxidation state of the central porphyrin core after having di-oxidized each branch of **4** will therefore dramatically reduce the kinetic stability of the resulting dececationic assembly. Also, several irreversible reduction waves are observed in scanning to more negative potentials, with that near -1.5 V possibly corresponding to the monoelectronic reduction of the ZnTPP core [47].

Table 1

Selected Optical and Redox Data for **2**-**4** [24,25].

Complex	UV-vis-NIR (CH_2Cl_2)	E° [M-based]	E° [TPP-based]
	λ_{max} nm (ε, 10^3 $M^{-1}.cm^{-1}$)	V *vs.* SCE [a, b]	
2	351 (34), 428 (330), 537 (16), 635 (15)	-0.14 (M = Fe) [c]	0.88[c]
2$[PF_6]_4$ [d]	338 (sh, 27), 431 (262), 555 (21), 587 (sh, 13), 682 (11), 778 (sh, 5)		
3	327 (93), 418 (364), 452 (sh, 97), 563 (31), 615 (39)	0.49 (M = Ru) [e]	0.87, 1.16 [e]
4	240 (sh, 227), 278 (sh, 118), 334 (93), 420 (368), 562 (26), 612 (32)	0.18 (M = Fe)	
4$[PF_6]_4$ [f]	248 (257), 319 (99), 422 (197), 565 (65), 605 (61), 644 (sh, 23), 1591 (31), 2290 (32)	0.76 (M = Ru)	≈ 0.9 [g]
4$[PF_6]_9$ [f]	250 (258), 360 (66), 448 (147), 584 (29), 658 (31), 1134 (95)	≈ 1.4[g] (M = Ru)	≈ 1.2 [g]

[a] Redox Potential. Conditions: CH_2Cl_2, 0.1 M [*n*-Bu_4N][PF_6], scan rate: 0.1 V s^{-1}. [b] E° [FcH^+/FcH] = 0.46 V [27]. [c] See ref. [24]. [d] Isolated tetracation. [e] See ref. [25]. [f] Species generated *in situ* by spectroelectrochemistry at -40 °C in the presence of [*n*-Bu_4N][PF_6] (0.3 M). [g] Tentative assignment.

*3.3. Spectroelectrochemistry of **2**, **3** and **4***

The spectroelectrochemistry of these compounds was also investigated. Isosbestic points consistent with fully reversible behaviour were obtained for the formation of the tetracation **2**$[PF_6]_4$, the redox state of compound **2** featuring oxidized organoiron substituents (Figure 3). As can be seen in Figure 3a, when the potential of the grid of the OTTLE cell is set at 0.5 V, only moderate changes take place in the electronic spectrum as the sample is oxidized. Thus, the Soret band at 23365 cm^{-1} (428 nm) and the Q-bands of the porphyrin core at 18620 cm^{-1} (537 nm) and 15750 cm^{-1} (635 nm) are red-shifted to lower energy by 160 cm^{-1}, 605 cm^{-1} and 1085 cm^{-1}, respectively, while the MLCT band near 28490 cm^{-1} (351 nm) disappears and a new band appears near 35100 cm^{-1} (285 nm). New MLCT bands might also appear at lower energy than the Soret band and might be overlapped with the Q bands [44]. Related observations have also been reported for some [ZnDPP] conjugates featuring a [Fe(κ^2-dppe)(η^5-C_5Me_5)(C≡C)] substituent [23]. A closer examination (Figure 3b) reveals that a very weak band also appears near 12600 cm^{-1} (793 nm) as a shoulder on the lower energy Q-band. The latter might be associated with the LMCT band often observed in Fe(III) [Fe(C≡CAr)(κ^2-dppe)(η^5-C_5Me_5)] metal-alkynyl complex cations [23,48]. A similar electronic spectrum was obtained in the UV-vis range for the isolated tetracationic species **2**$[PF_6]_4$ [24]. This cationic species was characterized in solution by NMR spectroscopy (Supporting Information) as being an open shell tetraradical with four apparently uncoupled electrons, one at each Fe(III) center [49]. The negligible electronic coupling between these unpaired electrons is supported by the ESR spectrum (Figure 4) [48], the resolved rhombic structure being diagnostic of non-coupled electrons for such polyradicals [50,51]. This confirms that the kinetically stable tetranuclear Fe(III) species can be cleanly (and reversibly) accessed by electrochemical means from **2** in the OTTLE cell. Consistent with the observation of a single Fe(II/III) oxidation process in the cyclic voltammogram, no transient extra band that might have corresponded to an intervalence charge transfer (IVCT) transition [52] between the peripheral organometallic [Fe(C≡CAr)(κ^2-dppe)(η^5-C_5Me_5)]- substituents was detected during the oxidation process. This indicates that if such processes exist, the peripheral redox groups are too weakly coupled through the ZnTPP core in the corresponding mixed valent (MV) states to give rise to intense IVCT bands. This contrasts with related metallated porphyrins such as **5** (Scheme 3), in which ferrocenyl redox-active endgroups are directly linked to the TPP core [53].

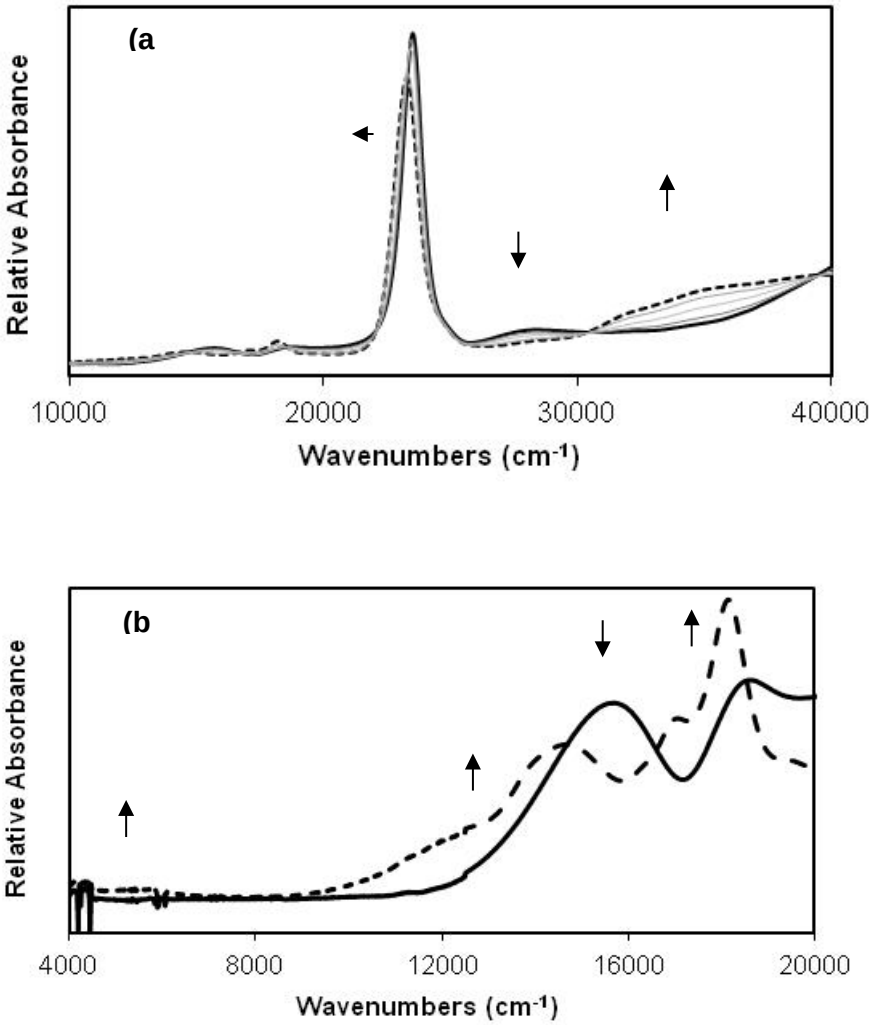

Fig. 3. (a) Spectroelectrochemistry of compound **2** (tetra-oxidized state shown with dotted line). (b) Detail of the near-IR/visible range. Conditions: CH_2Cl_2, 20 °C, [*n*-Bu_4N][PF_6] 0.3 M, starting potential: -0.5 V, applied potential: 0.8 V *vs.* AgCl/Ag reference electrode.

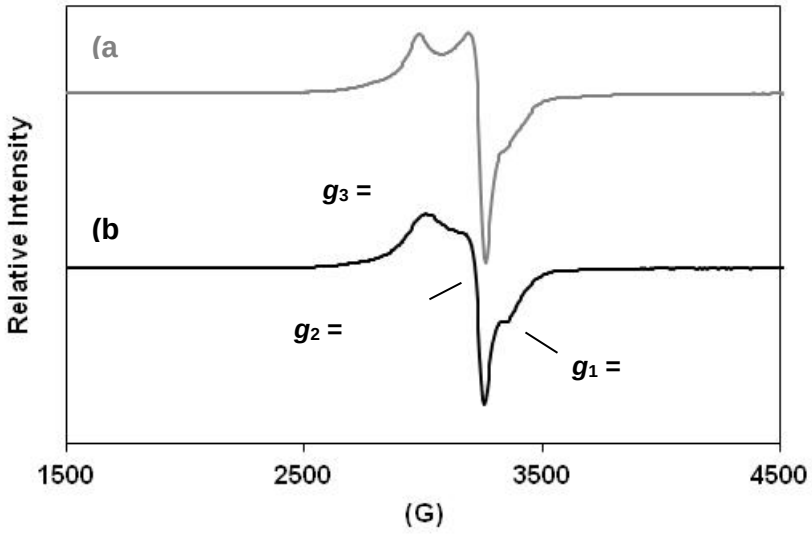

Fig. 4. a) ESR spectrum of **2**$[PF_6]_4$ generated *in situ* from **2** and [FcH][PF_6] (> 4 eq.) in THF glass at 70 K. b) ESR spectrum of isolated **2**$[PF_6]_4$ in CH_2Cl_2/1,2-$C_2H_4Cl_2$ (1:1) glass at 70 K.

In contrast to the complete chemical reversibility observed for **2**, the oxidation of **3** in the OTTLE cell was not fully reversible, since the spectrum of the neutral starting complex **3** could not be fully restored after the oxidation-reduction cycle (Supporting Information). Thus, we did not pursue investigations with **3** any further. Note, however, that the changes in the UV-vis region of the spectrum resulting from oxidation were less pronounced than observed with **2**, while qualitatively similar changes were observed in the near-IR region of the spectrum (except for the sharp decrease in reversibility).

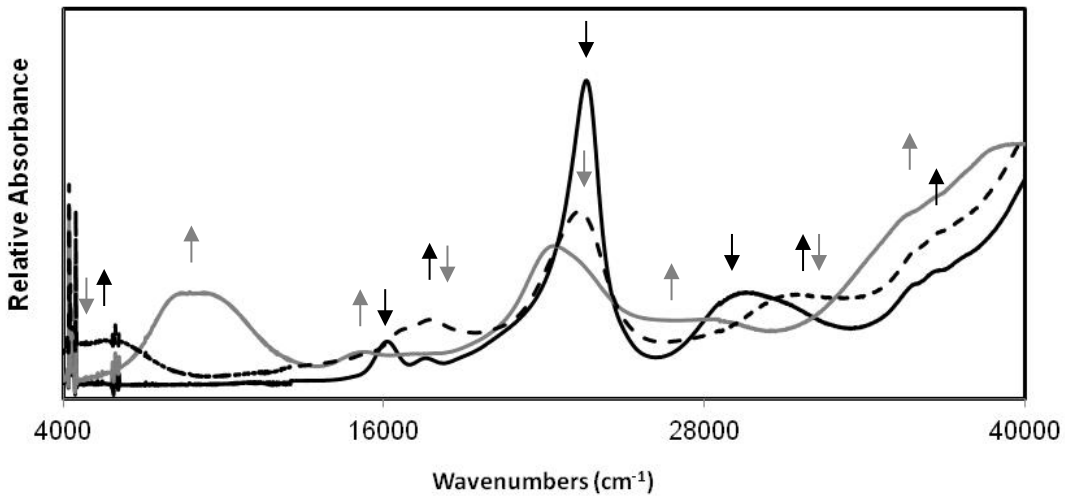

Fig. 5. UV-vis-NIR spectroelectrochemistry of **4** (tetra-oxidized state shown with dotted line and nonaoxidized state with grey line). Conditions: CH_2Cl_2, -40 °C, [*n*-Bu_4N][PF_6] 0.3 M, starting potential: -0.4 V, applied potentials: 0.4, 1.0 *vs.* SCE.

Finally, the new nonanuclear porphyrin derivative **4** was subjected to oxidation in the OTTLE cell. The temperature was lowered to avoid any unwanted side-reaction of the presumedly very reactive $\mathbf{4}^{9+}$ species; as a result, the starting spectrum could be fully restored after back-reduction. Setting the potential of the grid at 0.44 V afforded the first oxidized state, which most likely corresponds to the tetracation **4**$[PF_6]_4$ with four oxidized ferrocenium endgroups [20]. As a result, the Soret band at 23809 cm^{-1} (420 nm) and the two Q-bands at 17795 cm^{-1} (562 nm) and 16340 cm^{-1} (612 nm) in **4** are not significantly shifted, but the intensity of the second band increases significantly upon oxidation, most likely because of the presence of new underlying transitions (Figure 5). More marked is the hypsochromic shift of the band at 29940 cm^{-1} (334 nm) for **4**, which now appears at 31350 cm^{-1} (319 nm) in **4**$[PF_6]_4$; this is possibly due to the blue shift of the ferrocene-based contribution to this band upon oxidation of the ferrocenyl endgroups [42]. Likewise, new absorptions at 15530 cm^{-1} (644 nm), extending beneath the Q-bands, and also at 6285 cm^{-1} (1591 nm) have appeared. These transitions can be associated with oxidation of the ferrocenyl endgroups in the four [*trans*-Ru(κ^2-dppe)$_2$(C≡CFc){C≡C(1,4-C_6H_4)}]- branches, as previously seen with a specially designed model compound [20]. The lowest-energy band most likely corresponds to IVCT within each branch, while the 15530 cm^{-1} band likely corresponds to a charge transfer transition [54]. Further oxidation by setting the grid of the OTTLE cell at 1.0 V affords the

second oxidized state; this most likely corresponds to the polycation **4**$[PF_6]_9$, for which all four arms have been formally dioxidized along with a mono-oxidized central $[ZnTPP]^{\bullet+}$ core. The two intense bands located at 22320 cm^{-1} (448 nm) and 8820 cm^{-1} (1134 nm) are diagnostic of the presence of four [*trans*-Ru(κ^2-dppe)$_2$(C≡CFc){C≡C(1,4-C_6H_4)}]$^{2+}$- dicationic branches [20], while the disappearance of the Soret band (which is probably masked by the strong absorption at 22320 cm^{-1}) might be attributed to the radical cationic nature of the central ZnTPP core. Indeed, not much is known about the optical absorptions of such cores [46,55], but a decrease in intensity of the Soret band and broadening of the Q-bands in the 14280-18180 cm^{-1} (550-700 nm) range have been reported upon oxidation of divalent metal porphyrin derivatives [46,56]. Again, no transient extra band that might correspond to an IVCT transition between the peripheral organometallic substituents could be detected at any stage during the oxidation process, consistent with a weak (or negligible) electronic coupling of the peripheral organometallic groups through the ZnTPP core in the various MV states [53,57].

In terms of redox switching (or modulation) of the NLO properties, **4** appears to be a much more promising candidate than **2**, because the spectra of its redox isomers are more distinct from each other and from that of the starting complex. It is noteworthy that new and intense absorptions are produced in clearly distinct spectral ranges, such as the IVCT transitions observed in the near IR range for **4**$[PF_6]_4$ or the two specific transitions of the dicationic arms for **4**$[PF_6]_9$. At the wavelength of these transitions, optimal switching efficiencies of the cubic NLO effects might be obtained, based on results previously obtained with related heterobinuclear complexes, such as **6** (Scheme 3) [19].

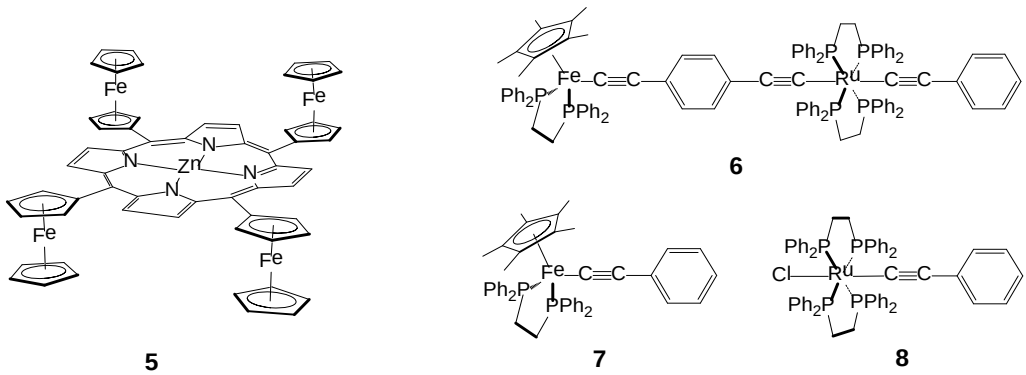

Scheme 3. Selected Compounds.

*3.4. Z-scan measurements of **4***

Third-order nonlinearities of **4** were determined by Z-scan studies at 560 nm and 630 nm, the results being listed in Table 2. These two wavelengths correspond to the wavelengths of the Q-bands of **4**. Although significant absorption occurs at these wavelengths, the γ value is dominated by the real part (γ_{real}) and not by the imaginary part (γ_{im}), emphasizing the importance of refractive over absorptive effects for this complex in this wavelength region. The cubic nonlinearity of **4** can be compared to those previously determined for the model complexes **7** and **8** (Scheme 3) at 695 nm and 800 nm, respectively [7]. Although assessed at different wavelengths, there is a *ca.* three orders of magnitude increase in the resulting γ value, confirming the importance of the extended π-manifold of **4** on the cubic nonlinearity. Table 2 also includes the (effective) two-photon absorption (TPA) cross-sections (σ_{2eff}) [10]. A significant increase is noted compared to the TPA cross-sections of the model alkynylmetal complexes **7** and **8**, but this is not so surprising considering that the cross-sections for **4** have been assessed at wavelengths where there is linear absorption, which necessitates caution in interpretation of the data (these cross-sections are actually "effective" cross-sections which most likely result from a combination of TPA, saturable absorption (SA) and reverse saturable absorption (RSA) [17]). These particular third-order NLO effects have considerable importance for the possible application in molecular-based devices for all-optical information encoding [58] or optical limiting [11]. Viewed from this perspective, the fact that positive values are found for **4** at 630 nm whereas negative values have previously been found for the related **2** and **1-X** derivatives (Scheme 1) at the wavelength of the second Q-band is noteworthy [24,25]. We cautiously suggest that TPA and RSA may dominate over SA effects at this wavelength for **4**, in contrast to **2** and **1-X** (X= NO_2, H, OMe). This differing behavior warrants a more in-depth investigation of these compounds to better understand the molecular origin of this particular change; studies directed towards this goal are currently underway.

Table 2

Experimental Cubic Nonlinear Optical Response Parameters. [a]

Complex	λ [b]	γ_{real} [c]	γ_{imag} [c]	$\lvert\gamma\rvert$ [c]	σ_2 [d]	Refs.
2	570	110 ± 10	21 ± 3	112 ± 10	6600 ± 1000	[24]

	650	/ [e]	/ [e]	/ [e]	-6100 ± 1000	[24]
4	560	-1030 ± 370	37.1 ± 17	1030 ± 370	18400 ± 8200	This work
	630	-710 ± 130	5.7 ± 1.8	710 ± 130	2240 ± 650	This work
7	695	0.11 ± 0.10	0.017 ± 0.01	0.11 ± 0.10	6 ± 3	[59]
8	800	-0.17 ± 0.04	0.071 ± 0.02	0.18 ± 0.045	/	[22]

[a] Conditions: measurements were carried out in CH_2Cl_2; γ values are referenced to the nonlinear refractive index of silica $n_2 = 2.92 \times 10^{-16}$ cm^2.W^{-1}. [b] Wavelength of the laser in nm. [c] 10^{-33} esu. The SI units for γ are C.m^4.V^{-3}, while those in the cgs system (used almost exclusively in the literature, and so given here) are cm^5.statV^{-2} or esu. To convert between the two systems, $\gamma_{SI} = (1/3)^4 \times 10^{-23}\ \gamma_{cgs}$. [d] Effective two-photon absorption cross-sections in Göppert-Mayer units, the conventional unit for TPA in the literature (1 GM = 1×10^{-50} cm^4.s^{-1}). [e] Not determined because of large one-photon absorption.

4. Conclusion

We have reported the synthesis and characterization of a new nonanuclear heterometallic molecular architecture of C_4 symmetry (**4**). The latter was obtained in one step by attaching four alkynylferrocene moieties to a tetraruthenium Zn(II) tetraphenyl porphyrin precursor (**3**). The electrochromic properties of **4** were investigated, together with those of the related organometallic porphyrin derivatives **2** and **3**, which feature metal alkynyl complexes as peripheral substituents. Amongst these redox-active systems, kinetically stable redox isomers of only **2** and **4** can be reversibly accessed *via* electrochemistry. Unfortunately, the electronic spectra of **2** and $\mathbf{2}^{4+}$ are dominated by ZnTPP-based transitions that are not strongly affected by oxidation of the peripheral organometallic substituents. Thus, quite similar linear optical signatures are found for the tetracation $\mathbf{2}^{4+}$ and for the starting compound **2**, suggesting only a weak redox modulation of the third-order NLO effects. In contrast, the new system **4** gives rise to two redox isomers with distinctly different linear optical signatures: the tetracation $\mathbf{4}^{4+}$ generated first upon oxidation, and the nonacation $\mathbf{4}^{9+}$, formed upon further oxidation. The tetracation $\mathbf{4}^{4+}$ presents new absorptions in a clearly distinct range (near-IR) from those of **4** assigned to IVCT and CT transitions within the heterobinuclear arms of the compound, while the nonacation $\mathbf{4}^{9+}$ also has a dramatically different electronic spectrum due to the oxidation of the central ZnTPP core along with the dioxidation of each arm. Such compounds offer interesting

perspectives for modulation of absorptive cubic NLO effects within three redox-accessible states at several wavelengths. Consistent with its extended π-unsaturated structure, preliminary Z-scan studies of **4** at 560 nm and 630 nm reveal that refractive effects dominate its cubic NLO behaviour (as given by the molecular γ value) and highlight an interesting nonlinear absorptive effect at 630 nm. Indeed, compared to the related compounds **1**-**X** and **2** which possess a dominant SA behavior at the wavelength of their second Q-band, the behavior of **4** is probably dominated by RSA or TPA. Studies are currently ongoing to better understand the molecular origin of this phenomenon and to further explore the potential of **4** and related compounds for redox modulation of the NLO properties.

Acknowledgments

F.P. and C.O.P.-R. thank the "Université Européenne de Bretagne" (UEB), the CNRS (PICS program N° 5676), and FEDER via an EPT grant in the "MITTSI" program from RTR BRESMAT for financial support. M.G.H. and M.P.C. thank the Australian Research Council for financial support, an Australian Professorial Fellowship (M.G.H.) and an Australian Research Fellowship (M.P.C.). A.M., N.R. and G.G. thank the "Région Bretagne" (ARED) for financial support. A. Bondon (ISCR/Rennes) is acknowledged for NMR support.

Appendix A. Supplementary data

Complementary experimental data for **4**, spectroelectrochemical traces for **3** and Z-scan plots for **4**. Supplementary data associated with this article can be found in the online version.

References

[1] S.R. Marder, Chem. Commun. (2006) 131-134.

[2] J.L. Brédas, C. Adant, P. Tackx, A. Persoons, Chem. Rev. 94 (1994) 243-278.

[3] P.N. Prasad, D.J. Williams, Nonlinear Optical Effects in Molecules and Polymers, John Wiley, New York, 1991.

[4] B. Luther-Davies, M. Samoc, Curr. Op. Solid State Mat. Sci. 2 (1997) 213-219.

[5] M. Samoc, J. Mol. Model. 17 (2011) 2183-2189.

[6] S. di Bella, C. Dragonetti, M. Pizzotti, D. Roberto, F. Tessore, R. Ugo, Top. Organomet. Chem. 28 (2010) 1-55.

[7] J.P. Morrall, G.T. Dalton, M.G. Humphrey, M. Samoc, Adv. Organomet. Chem. 55 (2008) 61-136.

[8] O. Maury, H. Le Bozec, Acc. Chem. Res. 38 (2005) 691-703.

[9] M. Pawlicki, H.A. Collins, R.G. Denning, H.L. Anderson, Angew. Chem. Int. Ed. 48 (2009) 3244-3266.

[10] G.S. He, L.-S. Tan, Q. Zheng, P.N. Prasad, Chem. Rev. 108 (2008) 1245-1330.

[11] M. Calvete, G.Y. Yang, M. Hanack, Synth. Met. 141 (2004) 231–243.

[12] M. Ravikanth, K.G. Ravindra, Curr. Sci. 68 (1995) 1010-1017.

[13] J.L. Humphrey, D. Kuciauskas, J. Phys. Chem. C 128 (2006) 3902-3903.

[14] S.V. Rao, N.K.M.N. Srinivas, D.N. Rao, L. Giribabu, B.G. Mayia, R. Philip, G.R. Kumar, Optics Commun. 182 (2000) 255-264.

[15] N.J. Long, Angew. Chem., Int. Ed. Engl. 34 (1995) 21-38.

[16] I.R. Whittall, A.M. McDonagh, M.G. Humphrey, M. Samoc, Adv. Organomet. Chem. 42 (1998) 291-362.

[17] I.R. Whittall, A.M. McDonagh, M.G. Humphrey, M. Samoc, Adv. Organomet. Chem. 43 (1999) 349-405.

[18] G. Grelaud, M.P. Cifuentes, F. Paul, M.G. Humphrey, J. Organomet. Chem. 751 (2014) 181-200.

[19] N. Gauthier, G. Argouarch, F. Paul, L. Toupet, A. Ladjarafi, K. Costuas, J.-F. Halet, M. Samoc, M.P. Cifuentes, T.C. Corkery, M.G. Humphrey, Chem. Eur. J. 17 (2011) 5561-5577.

[20] G. Grelaud, M.P. Cifuentes, T. Schwich, G. Argouarch, S. Petrie, R. Stranger, F. Paul, M.G. Humphrey, Eur. J. Inorg. Chem. (2012) 65–75.

[21] M.P. Cifuentes, C.E. Powell, M.G. Humphrey, G.A. Heath, M. Samoc, B. Luther-Davies, J. Phys. Chem. A 105 (2001) 9625-9627.

[22] C.E. Powell, M.P. Cifuentes, J.P. Morrall, R. Stranger, M.G. Humphrey, M. Samoc, B. Luther-Davies, G.A. Heath, J. Am. Chem. Soc. 125 (2003) 602-610.

[23] M. Murai, M. Sugimoto, M. Akita, Dalton Trans. 42 (2013) 16108-16120.

[24] S. Drouet, A. Merhi, G. Grelaud, M.P. Cifuentes, M.G. Humphrey, K. Matczyszyn, M. Samoc, L. Toupet, C.O. Paul-Roth, F. Paul, New J. Chem. 36 (2012) 2192-2195.

[25] S. Drouet, A. Merhi, D. Yao, M.P. Cifuentes, M.G. Humphrey, M. Wieglus, J. Olesiak-Banska, K. Matczyszyn, M. Samoc, F. Paul, C.O. Paul-Roth, Tetrahedron 68 (2012) 10351-10359.

[26] D.F. Shriver, M.A. Drezdzon, The Manipulation of Air-Sensitive Compounds, Wiley, New York, 1986.

[27] N.G. Connelly, W.E. Geiger, Chem. Rev. 96 (1996) 877-910.

[28] G. Doisneau, G. Balavoine, T. Fillebeen-Khan, J. Organomet. Chem., 425 (1992) 113-117.

[29] C.M. Duff, G.A. Heath, Inorg. Chem. 30 (1991) 2528-2535.

[30] M. Sheikh-Bahae, A.A. Said, T. Wei, D.J. Hagan, E.W. van Stryland, IEEE J. Quant. Electr. 26 (1990) 760-769.

[31] M. Samoc, A. Samoc, B. Luther-Davies, M.G. Humphrey, M.S. Wong, Opt. Mater. 21 (2003) 485-488.

[32] D. Touchard, P. Haquette, S. Guesmi, L. Le Pichon, A. Daridor, L. Toupet, P.H. Dixneuf, Organometallics 16 (1997) 3640-3648.

[33] G. Grelaud, N. Gauthier, Y. Luo, F. Paul, B. Fabre, F. Barrière, S. Ababou-Girard, T. Roisnel, M.G. Humphrey, J. Phys. Chem. C 118 (2014) 3680-3695.

[34] M.C. Colbert, J. Lewis, N.J. Long, P.R. Raithby, A.J.P. White, D.J. Williams, J. Chem. Soc., Dalton. Trans. (1997) 99-104.

[35] Z. Li, A.M. Beatty, S. Sharma, T.P. Fehlner, Inorg. Chem. 42 (2003) 5707-5714.

[36] S.K. Hurst, M.G. Humphrey, J.P. Morrall, M.P. Cifuentes, M. Samoc, B. Luther-Davies, G.A. Heath, A.C. Willis, J. Organomet. Chem. 670 (2003) 56-65.

[37] A.M. McDonagh, I.R. Whittall, M.G. Humphrey, D.C.R. Hockless, B.W. Skelton, A.H. White, J. Organomet. Chem. 523 (1996) 33-40.

[38] N. Gauthier, C. Olivier, S. Rigaut, D. Touchard, T. Roisnel, M.G. Humphrey, F. Paul, Organometallics 27 (2008) 1063-1072.

[39] A.M. McDonagh, C.E. Powell, J.P. Morrall, M.P. Cifuentes, M.G. Humphrey, Organometallics 22 (2003) 1402-1413.

[40] N. Gauthier, N. Tchouar, F. Justaud, G. Argouarch, M.P. Cifuentes, L. Toupet, D. Touchard, J.-F. Halet, S. Rigaut, M.G. Humphrey, K. Costuas, F. Paul, Organometallics 28 (2009) 2253-2266.

[41] M.A. Fox, J.E. Harris, S. Heider, V. Pérez-Gregorio, M.E. Zakrzewska, J.D. Farmer, D.S. Yufit, J.A.K. Howard, P.J. Low, J. Organomet. Chem. 694 (2009) 2350-2358.

[42] L. Cuffe, R.D.A. Hudson, J.F. Gallagher, S. Jennings, C.J. McAdam, R.B.T. Connelly, A.R. Manning, B.H. Robinson, J. Simpson, Organometallics 24 (2005) 2051-2060, and refs therein.

[43] E.S. Schmidt, T. S. Calderwood, T.C. Bruice, Inorg. Chem. 25 (1986) 3718-3720.

[44] V.N. Nemykin, R.G. Hadt, J. Phys. Chem. A 114 (2010) 12062–12066.

[45] M.C.C. Colbert, J. Lewis, N.J. Long, P.R. Raithby, M. Younus, A.J.P. White, D.J. Williams, N.J. Payne, L. Yellowlees, D. Beljonne, N. Chawdhury, R.H. Friend, Organometallics 17 (1998) 3034-3043.

[46] A. Wolberg, J. Manassen, J. Am. Chem. Soc. 92 (1970) 2982-2991.

[47] J. Rault-Berthelot, C.O. Paul-Roth, C. Pohriel, S. Julliard, S. Ballut, S. Drouet, G. Simonneaux, J. Electroanal. Chem. 623 (2008) 204–214.

[48] F. Paul, L. Toupet, J.-Y. Thépot, K. Costuas, J.-F. Halet, C. Lapinte, Organometallics 24 (2005) 5464-5478.

[49] F. Paul, G. da Costa, A. Bondon, N. Gauthier, S. Sinbandhit, L. Toupet, K. Costuas, J.-F. Halet, C. Lapinte, Organometallics 26 (2007) 874-896.

[50] S. Ibn Ghazala, F. Paul, L. Toupet, T. Roisnel, P. Hapiot, C. Lapinte, J. Am. Chem. Soc. 128 (2006) 2463-2476.

[51] G. Grelaud, O. Cador, T. Roisnel, G. Argouarch, M.P. Cifuentes, M.G. Humphrey, F. Paul, Organometallics 31 (2012) 1635−1642.

[52] F. Paul, C. Lapinte, Coord. Chem. Rev. 178/180 (1998) 431-509.

[53] G.T. Rohde, J.R. Sabin, C.D. Barrett, V.N. Nemykin, New J. Chem. 35 (2011) 1440-1448.

[54] F. Paul, work in progress.

[55] Z. Gasyna, W.R. Browett, M.J. Stillman, Inorg. Chem. 24 (1985) 2440-2447.

[56] G.M. Brown, F.R. Hopf, J.A. Ferguson, T.J. Meyer, D.G. Whitten, J. Am. Chem. Soc. 95 (1973) 5939-5942.

[57] V.N. Nemykin, G.T. Rohde, C.D. Barrett, R.G. Hadt, C. Bizzarri, P. Galloni, B. Floris, I. Nowik, R.H. Herber, A.G. Marrani, R. Zanoni, N.M. Loim, J. Am. Chem. Soc. 131 (2009) 14969-14978.

[58] F.Z. Henari, J. Opt. A: Pure Appl. Opt. 3 (2001) 188-190.

[59] M.P. Cifuentes, M.G. Humphrey, J.P. Morrall, M. Samoc, F. Paul, T. Roisnel, C. Lapinte, Organometallics 24 (2005) 4280-4288.

Appendix A. Supplementary data

Areej Merhi,[a,b] *Guillaume Grelaud,*[a,c] *Nicolas Ripoche,*[a,c] *Adam Barlow,*[c] *Marie P. Cifuentes,*[c] *Mark G. Humphrey,*[*,c] *Frédéric Paul*[*,a] *and Christine O. Paul-Roth*[*,a]

A Zinc(II) Tetraphenylporphyrin Peripherally Functionalized with Redox-Active "*trans*-[(η^5-C_5H_5)Fe(η^5-C_5H_4)C≡C](κ^2-dppe)$_2$Ru(C≡C)-" Substituents: Linear Electrochromism and Third-Order Nonlinear Optics

Including:

1. Labelling Scheme in NMR Spectral Assignments and ^{13}C NMR Spectrum

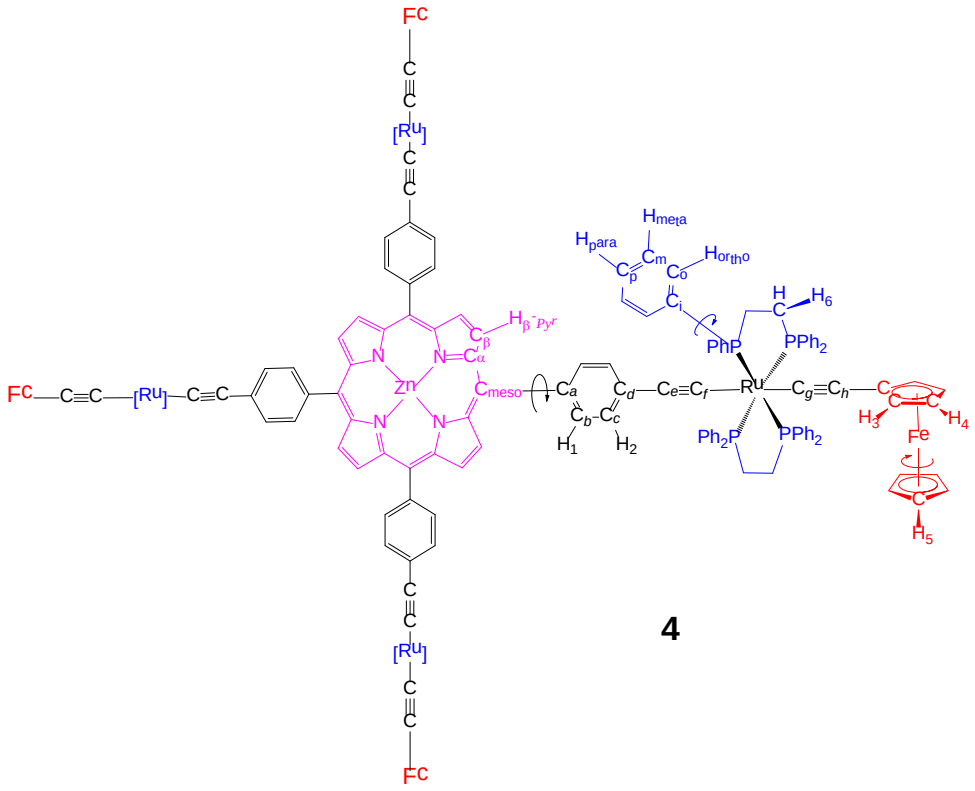

4

^{13}C{^{1}H} NMR (δ, 125 MHz, CD_2Cl_2): 150.6 (s, $C_{\alpha\text{-pyrrolic}}$), 137.7 (m, 2 $C_{ipso/dppe}$), 134.8 (m, 2 $CH_{ortho/Ph/dppe}$), 134.6 (s, $CH_{Ar}[C_b]$), 132.2 (s, $C_{\beta\text{-pyrrolic}}$), 130.1 (s, $C_{Ar}[C_d]$), 129.1 & 129.0 (s, $CH_{para/Ph/dppe}$), 128.5 (s, $CH_{Ar}[C_c]$), 127.5 & 127.3 (s, $CH_{meta/Ph/dppe}$), 123.0 (s, C_{meso}), 116.9 (s, RuC≡C[C_e]), 112.6 (s, RuC≡C[C_h]), 78.3 (s, $C_{CpC\equiv C}$), 70.2 (s, $CH_{CpC\equiv C}$), 70.0 (s, C_5H_5), 67.5 (s, $CH_{CpC\equiv C}$), 33.1 (m, $CH_{2/dppe}$); 2 RuC≡C [$C_{f\text{-}g}$] and 1 $C_{Ar}[C_a]$ not observed, possibly overlapped. Proposed attribution based on HMBC and HMQC-type polarization transfer.

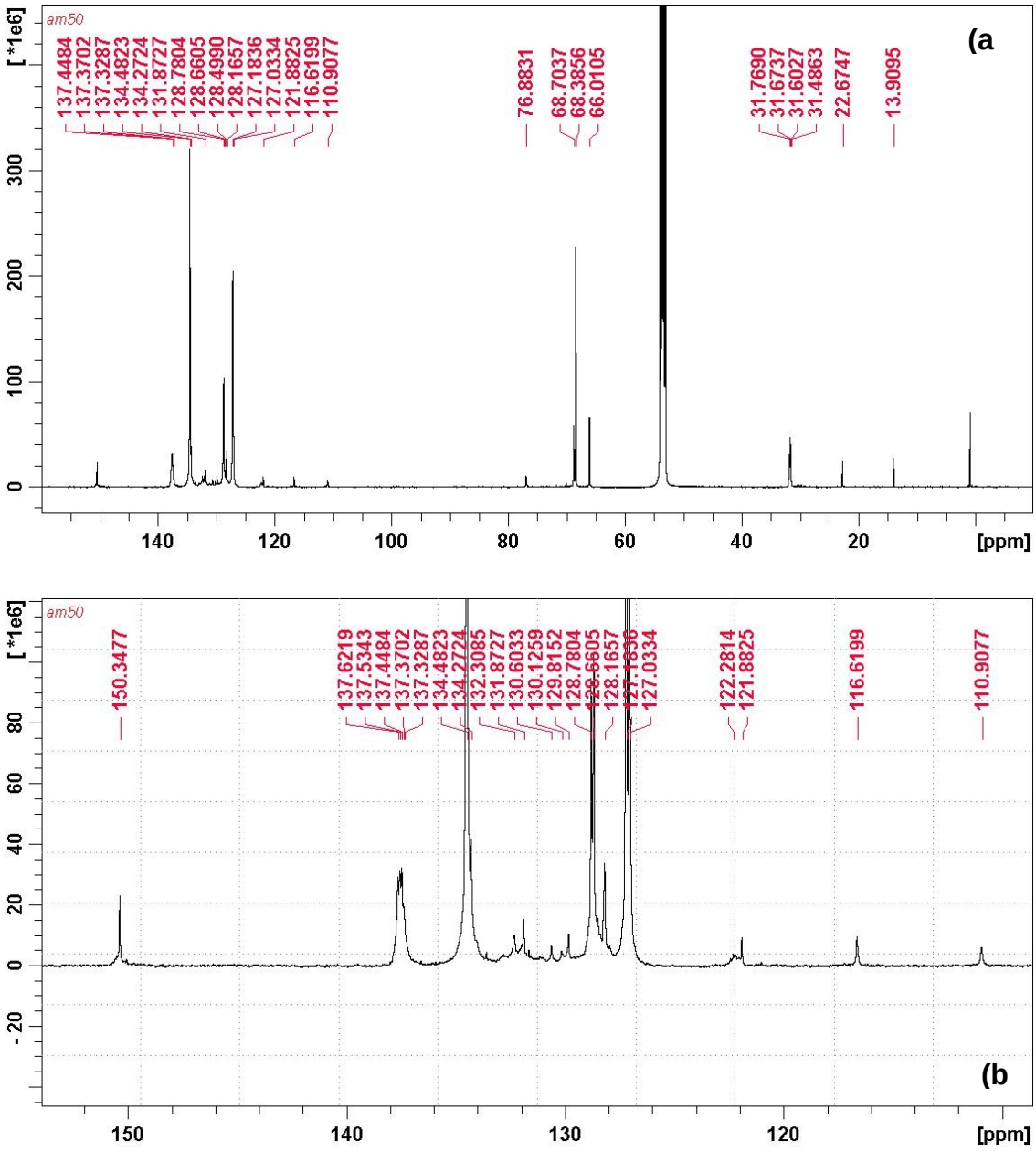

Fig. S1. (a) Full ^{13}C NMR spectrum of **4** in CD_2Cl_2 at 300 K. (b) Expanded part of spectrum (a).

2. Cyclic Voltammogram of 4

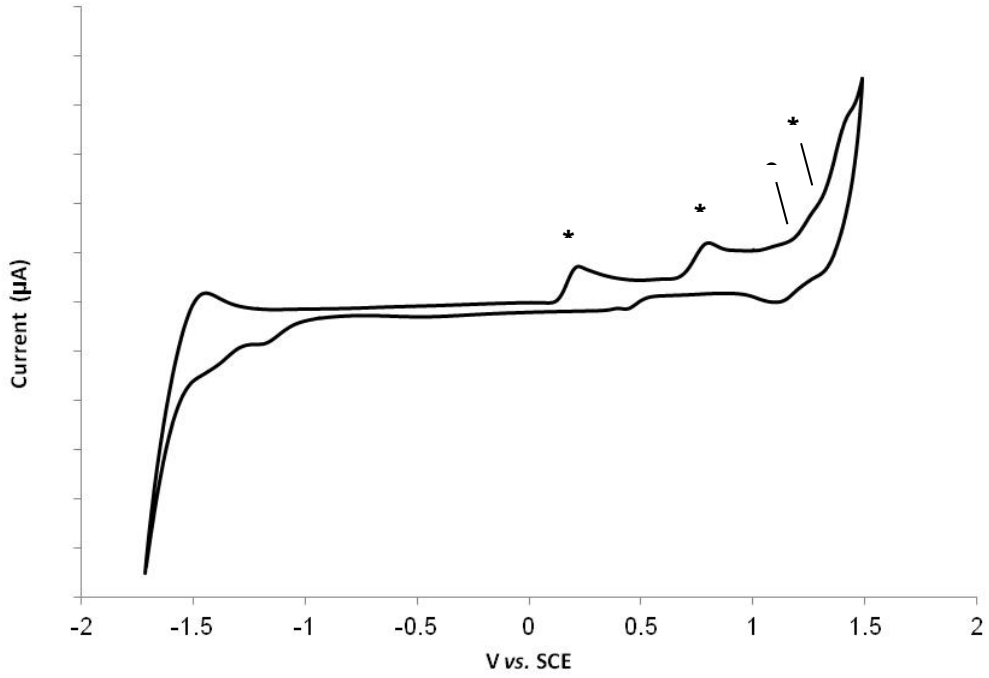

Fig. S2. Cyclic voltammogram of compounds **4** in the -1.8 V/1.6 V range, showing the Fe- and Ru-centered redox processes and another intense redox event (*). The second oxidation of the ZnTPP core is indicated by a dot (●). Conditions: CH_2Cl_2, 20 °C, [*n*-Bu_4N][PF_6] 0.1 M, scan rate: 0.1 V/s. Potential values given *vs.* SCE.

3. ^{1}H NMR Spectrum of 2[PF$_6$]$_4$

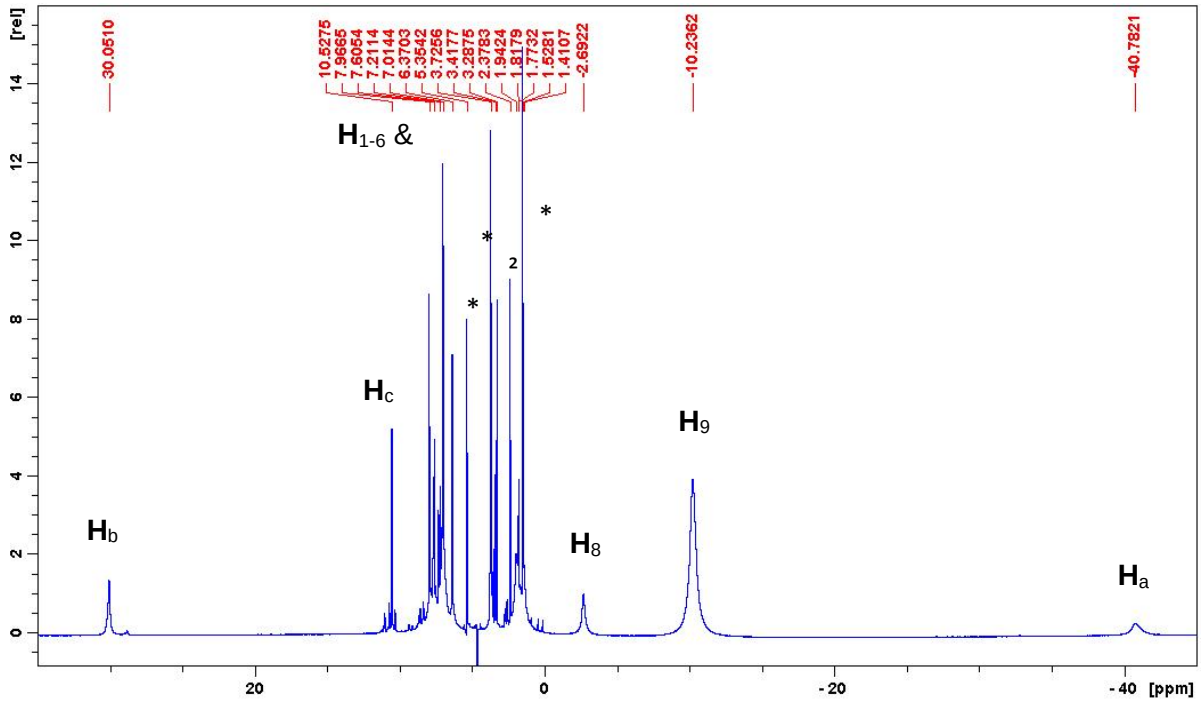

Fig. S3. ^{1}H NMR spectrum of **2**[PF$_6$]$_4$ in CD_2Cl_2 at 300 K. Numbering of selected protons according to Chart S1 (below). Signals corresponding to solvents are designated by asterisks (*).

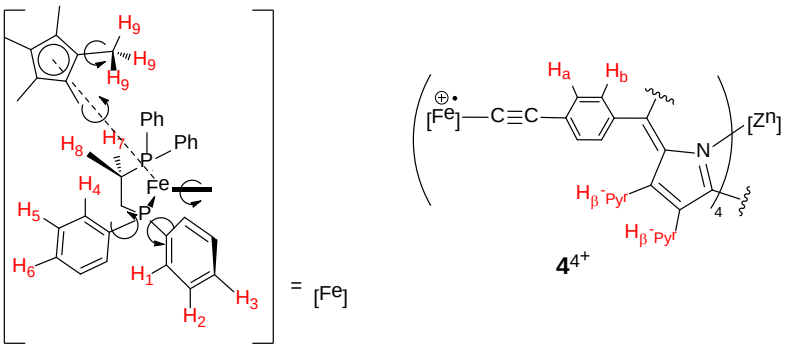

Chart S1. ^{1}H nuclei numbering corresponding to the proposed assignment for **2**[PF$_6$]$_4$.

4. Spectroelectrochemistry of 3

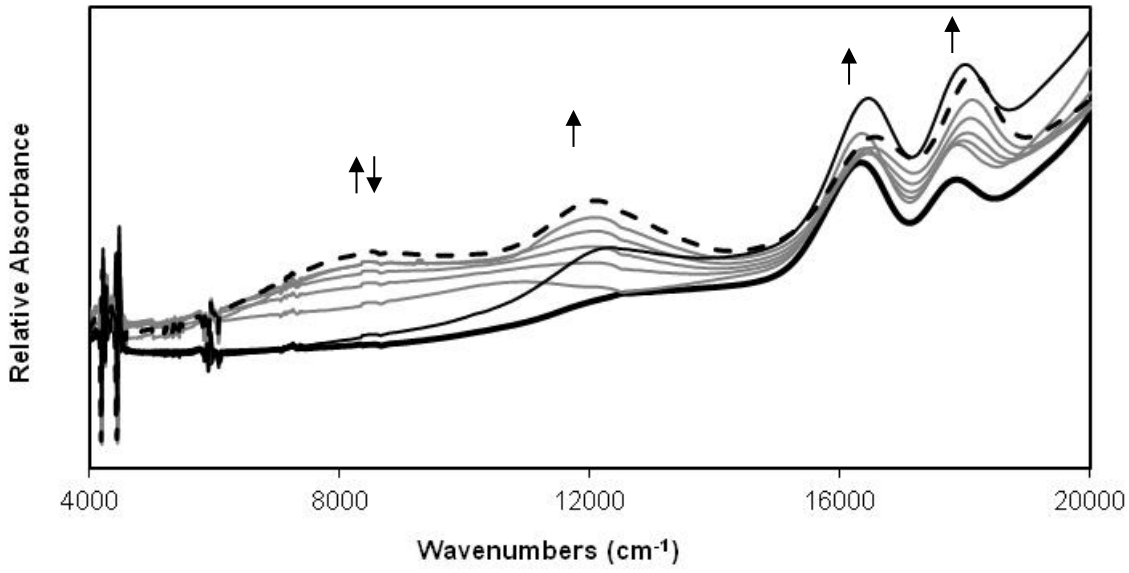

Fig. S4. Spectroelectrochemistry of compound **3**. The oxidized state is shown with a dotted line and the state recovered after back-reduction is given with a thin black line. Conditions: CH_2Cl_2, 20 °C, [*n*-Bu_4N][PF_6] 0.3 M, starting potential: -0.6 V, applied potential: 0.9 V *vs.* SCE. The region of the spectrum to higher energy of 20,000 cm^{-1} is only marginally affected by redox changes.

5. Z-Scan Plots for 4

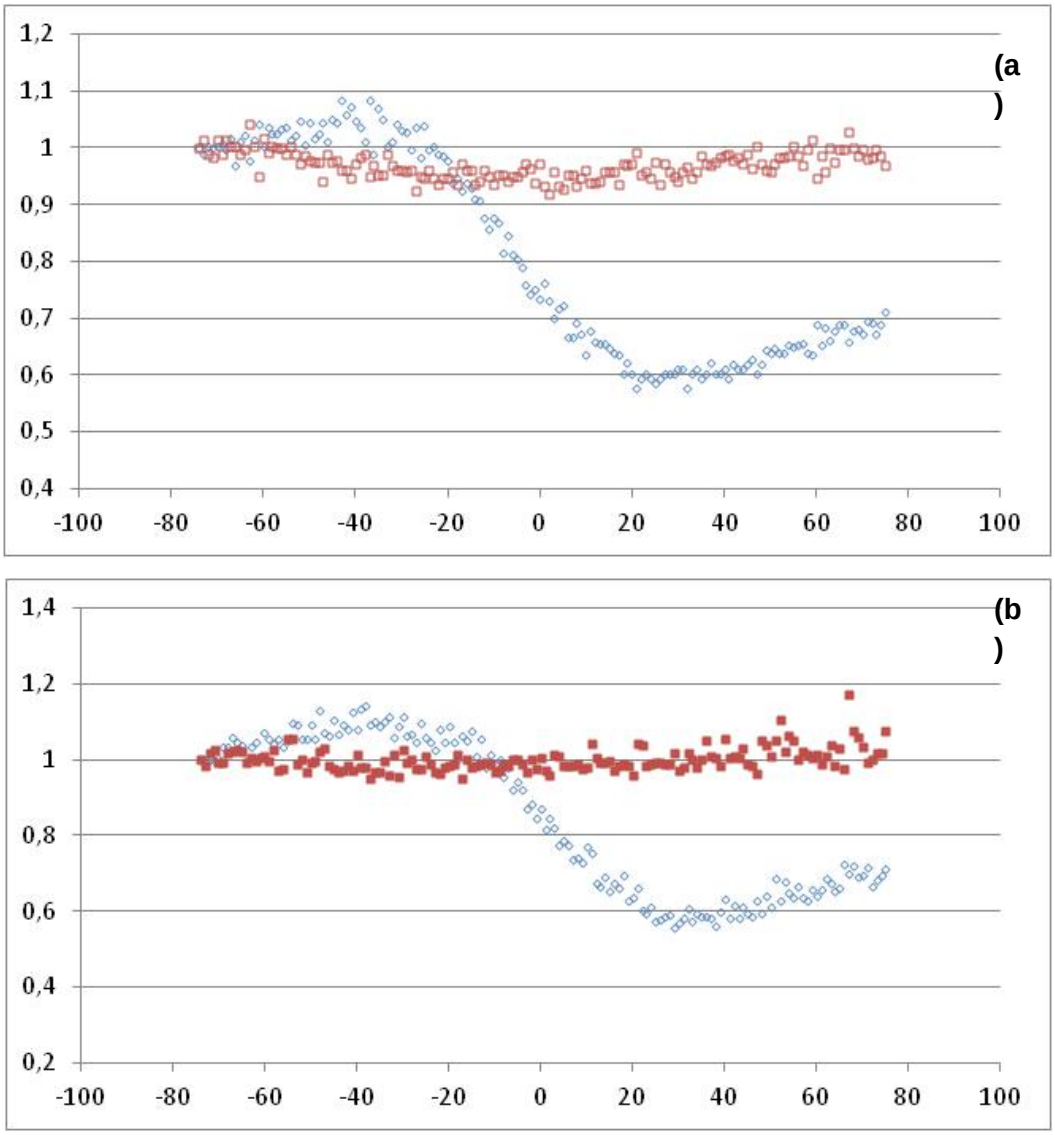

Fig. S4. Z-scan plots obtained for compound **4** at 560 nm (a) and 630 nm (b). Blue: closed-aperture traces. Red: open-aperture traces.